arXiv:1403.5512v1 [hep-ph] 21 Mar 2014

Jet substructures of boosted polarized top quarks

Yoshio Kitadono[1*] and Hsiang-nan Li[1,2,3†]

[1]*Institute of Physics, Academia Sinica,*

Taipei 11529, Taiwan, Republic of China

[2]*Department of Physics, National Cheng-Kung University,*

Tainan, Taiwan701, Republic of China and

[3]*Department of Physics, National Tsing-Hua University,*

Hsin-Chu, Taiwan300, Republic of China

(Dated: March 24, 2014)

Abstract

We study jet substructures of a boosted polarized top quark, which undergoes the semileptonic decay $t \to b\ell\nu$, in the perturbative QCD framework. The jet mass distribution (energy profile) is factorized into the convolution of a hard top-quark decay kernel with the bottom-quark jet function (jet energy function). Computing the hard kernel to leading order in QCD and inputting the latter functions from the resummation formalism, we observe that the jet mass distribution is not sensitive to the helicity of the top quark, but the energy profile is: energy is accumulated faster within a left-handed top jet than within a right-handed one, a feature related to the $V-A$ structure of weak interaction. It is pointed out that the energy profile is a simple and useful jet observable for helicity discrimination of a boosted top quark, which helps identification of physics beyond the Standard Model at the Large Hadron Collider. The extension of our analysis to other jet substructures, including those associated with a hadronically decaying polarized top quark, is proposed.

PACS numbers: 14.65.Ha, 13.88.+e, 12.38.Cy, 13.87.-a

*Electronic address: kitadono@phys.sinica.edu.tw

†Electronic address: hnli@phys.sinica.edu.tw

I. INTRODUCTION

The precise theoretical and experimental investigation of top-quark properties [1–3] is crucial not only for understanding the electroweak dynamics in the Standard Model, but also for exploring new physics beyond the Standard Model. Especially, information of the top-quark polarization can reveal the chiral structure of new physics. To translate the chiral couplings of a top quark to new physics into observable polarization signals, the top quark must be sufficiently boosted, as chirality is equivalent to helicity in the massless limit. A top quark may be produced with large boost at the Large Hadron Collider (LHC) in the future 14 TeV run, for example, directly through the quark and antiquark annihilation, or indirectly through the decay of a new massive particle. The final states of a boosted top quark then become collimated and form a single jet. The polarization of a top quark, if produced at rest, is determined by measuring the angular distribution of decay products (see [4, 5] and references therein). Such measurement is not feasible even for the final-state lepton with the largest spin analyzing power, as a top quark is highly boosted.

Fixed-order calculations and soft-gluon resummations associated with the boosted top quark production have been performed in the Standard Model [6–9]. Exploration of new physics beyond the Standard Model by means of boosted top quarks was studied intensively in [10–19]. Various strategies for tagging a boosted top quark were proposed in [20–27], and experimental searches have been conducted by ATLAS and CMS recently [28, 29]. The relation between the polarization of a boosted top quark and the energy fraction distribution of a particular subjet was discussed in [30] using Monte Carlo generators. Given an algorithm for the subjet selection, different energy fraction distributions for the left- and right-handed top jets have been noticed. It implies that jet substructures can serve as observables for distinguishing the helicity of a boosted polarized top quark. In this paper we shall demonstrate in the perturbative QCD (pQCD) framework that the energy profile of a top jet is a simple and useful substructure for this purpose without requiring decomposition of subjets and algorithms for subject selection as in [30], b-tagging, W-reconstruction or measurement of missing momentum.

We start with the jet function of a polarized leptonic top, which undergoes the $t \to b\ell\nu$ decay as an example. In pQCD this function is factorized into the convolution of a hard top-quark decay kernel with the bottom-quark jet function. The latter can be well approximated

by the light-quark jet function [31] derived in the QCD resummation formalism [32], as the jet energy is high enough. Evaluating the hard kernel to leading order (LO) in QCD, we obtain the dependencies of the left- and right-handed top-quark jet functions on the top-jet momentum and cone radius. It is found that the top-quark jet function is not sensitive to the helicity as expected, since its peak position is basically determined by the top-quark mass. The similarity of the jet functions implies the similarity of the mass distributions of the left- and right-handed top jets. Hence, boosted top candidates can be identified by means of the jet mass measurement, together with other promising techniques available in the literature. Certainly, the mass measurement demands reconstruction of a missing neutrino momentum, which we do not intend to explore further. The essence is that additional information on the internal structure of a top jet is required in order to distinguish its helicity.

After practicing the factorization of the top-quark jet function, we extend it to the top-jet energy profile [33]

$$\Psi(r) \;=\; \frac{1}{N_{J_t}} \sum_{J_t} \frac{\sum_{r_i<r, i\in J_t} P_{T_i}}{\sum_{r_i<R_t, i\in J_t} P_{T_i}}, \tag{1}$$

where N_{J_t} is the number of top jets with cone radius R_t, $r \leq R_t$ is the radius of a test cone centered around the top-jet axis, P_{T_i} is the transverse momentum carried by particle i in the top jet J_t. The lepton energy is not included in $\Psi(r)$, and the neutrino energy, as a missing momentum, does not contribute either. This observable is then expressed as the convolution of a hard top-quark decay kernel with the bottom-quark jet energy function. Inputting the light-quark jet energy function derived also from the QCD resummation [32], we predict the energy profiles of the left- and right-handed top jets. It turns out that the energy profile is sensitive to the helicity: energy is accumulated faster within a left-handed top jet than within a right-handed one, a feature related to the $V - A$ structure of weak interaction. The dependencies of the energy profiles of the left- and right-handed top jets on the top-jet momentum and cone radius are presented for future experimental confrontation.

Our work does not only represent an application of pQCD to the study of jet substructures of a boosted weakly decaying massive particle, but also highlights the energy profile as a simple and useful observable for distinguishing the helicity of a boosted top quark. The pQCD factorization formulas for the jet function and the jet energy function of a polarized leptonic top are constructed in Sec. II. The sensitivity of the top-jet mass distribution and energy profile to the helicity is examined numerically in Sec. III. Section IV is the conclusion.

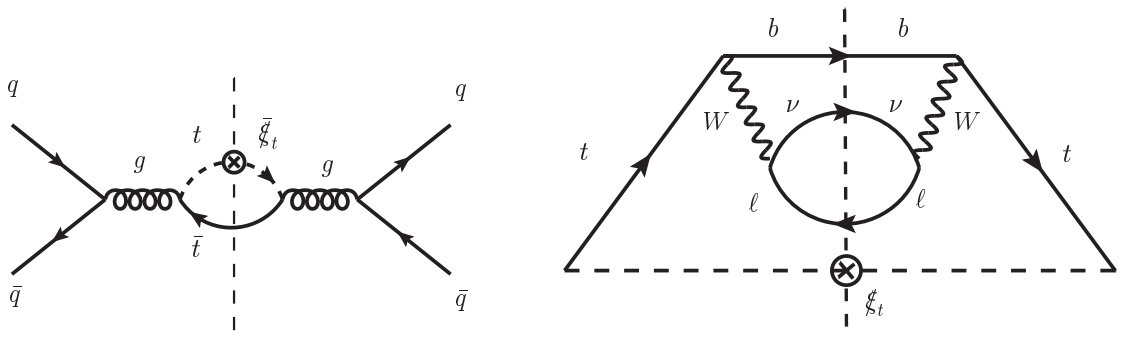

(a) (b)

FIG. 1: LO diagrams for (a) the production and (b) the semi-leptonic decay of a top quark. The dashed lines label the fermion flows, and the symbols $\otimes$ represent the insertions of the gamma matrices $\bar{\not{\xi}}_t$ and $\not{\xi}_t$ from the Fierz identity.

II. FORMALISM

We consider only the annihilation $q\bar{q} \to t\bar{t}$ as the production process for simplicity in order to demonstrate the construction of the top-quark jet function J_t. The factorization at LO in QCD is trivial, which requires only the insertion of the Fierz identity to break the fermion flow,

$$\mathbf{1}_{ij}\mathbf{1}_{lk} = \frac{1}{4}\mathbf{1}_{ik}\mathbf{1}_{lj} + \frac{1}{4}(\gamma^5)_{ik}(\gamma^5)_{lj} + \frac{1}{4}(\gamma_\alpha)_{ik}(\gamma^\alpha)_{lj} + \frac{1}{4}(\gamma^5\gamma_\alpha)_{ik}(\gamma^\alpha\gamma^5)_{lj} + \frac{1}{8}(\sigma_{\alpha\beta})_{ik}(\sigma^{\alpha\beta})_{lj}, \tag{2}$$

with the identity matrix $\mathbf{1}$, and i, j, k, and l being the Dirac indices. We introduce the light-like vectors [31]

$$\xi_t^\alpha \equiv \frac{1}{\sqrt{2}}(1, -\vec{n}_t), \qquad \bar{\xi}_t^\alpha \equiv \frac{1}{\sqrt{2}}(1, \vec{n}_t), \tag{3}$$

to pick up the leading term in Eq. (2). The unit vector $\vec{n}_t$ denotes the direction of the top-quark momentum, which can be determined by measuring the hadronic anti-top in the $t\bar{t}$ system. At higher orders, QCD radiations from the final states, that are collinear to the top quark, are grouped into J_t straightforwardly. The collinear initial-state radiations are collected by the Wilson lines in the direction of ξ_t [32], which are associated with the definition of J_t.

The corresponding LO matrix element squared $\left|\overline{\mathcal{M}}\right|^2$ is then factorized, up to power corrections of $O(m_t/E_t)$, m_t (E_t) being the top-quark mass (energy), into two pieces, i.e.,

the production part $\left|\overline{\mathcal{M}}_{pro}\right|^2$ shown in Fig. 1(a) and the decay part $\left|\overline{\mathcal{M}}_{decay}\right|^2$ for a leptonic top in Fig. 1(b),

$$\begin{aligned}
\left|\overline{\mathcal{M}}\right|^2 &= \left|\overline{\mathcal{M}}_{pro}\right|^2\left|\overline{\mathcal{M}}_{decay}\right|^2\left[1+O\left(\frac{m_t}{E_t}\right)\right], \\
\left|\overline{\mathcal{M}}_{pro}\right|^2 &= \frac{1}{4}\frac{g_s^4 T_R C_F}{4N_c s^2}\mathrm{tr}\left(\gamma^\mu \not{k}\gamma^\rho \not{\bar{k}}\right)\mathrm{tr}\left[\gamma_\mu(\not{k}_{\bar{t}}-m_t)\gamma_\rho \not{\xi}_{\bar{t}}\right], \\
\left|\overline{\mathcal{M}}_{decay}\right|^2 &= C_{decay}\mathrm{tr}\left(\gamma^\gamma P_L \not{k}_\nu \gamma^\sigma P_L \not{k}_\ell\right)\mathrm{tr}\left[\gamma_\sigma P_L(\not{k}_t+m_t)\not{\xi}_t(\not{k}_t+m_t)\gamma_\gamma P_L(\not{k}_b+m_b)\right], \quad (4)
\end{aligned}$$

where the factor C_{decay} collects the W-boson and top-quark propagators

$$C_{decay} = \frac{g^4}{4}|V_{tb}|^2\frac{1}{(q_W^2-m_W^2)^2+m_W^2\Gamma_W^2}\frac{1}{(k_t^2-m_t^2)^2+m_t^2\Gamma_t^2}. \quad (5)$$

In the above expressions, g_s is the QCD coupling, $N_c=3$, $T_R=1/2$ and $C_F=4/3$ are the color factors, $\sqrt{s}$ is the center-of-mass energy of the $t\bar{t}$ system, g is the weak coupling, $|V_{tb}|$ is the Cabibbo-Kobayashi-Maskawa matrix element, k, $\bar{k}$, k_t, $k_{\bar{t}}$, k_b, k_ℓ, k_ν, and q_W are the momenta of the q quark, $\bar{q}$ quark, t quark, $\bar{t}$ quark, b quark, lepton, neutrino, and W boson, respectively, m_W and m_b are the masses of the W boson and b quark, respectively, Γ_W and Γ_t are the decay widths of the W boson and top quark, respectively, and $P_L=(1-\gamma^5)/2$ is the chiral projection matrix. The top-quark (anti-top-quark) line has been assigned to the decay (production) piece in the factorization.

Next we decompose the decay piece for the unpolarized top quark according to the spin states s_t by introducing the projectors

$$w_t = \frac{1}{2}(1+\gamma^5 \not{s}_t), \qquad \bar{w}_t = \frac{1}{2}(1-\gamma^5 \not{s}_t). \quad (6)$$

Equation (4) becomes

$$\begin{aligned}
\left|\overline{\mathcal{M}}_{decay}\right|^2 &= \left|\overline{\mathcal{M}}^{s_t}_{decay}\right|^2+\left|\overline{\mathcal{M}}^{\bar{s}_t}_{decay}\right|^2, \\
\left|\overline{\mathcal{M}}^{s_t}_{decay}\right|^2 &= 2C_{decay}(\xi_t\cdot k_t)\mathrm{tr}\left(\gamma^\gamma P_L \not{k}_\nu\gamma^\sigma P_L \not{k}_\ell\right)\mathrm{tr}\left[\gamma_\sigma P_L(\not{k}_t+m_t)w_t\gamma_\gamma P_L(\not{k}_b+m_b)\right] \\
&\quad +O(k_t^2-m_t^2), \\
\left|\overline{\mathcal{M}}^{\bar{s}_t}_{decay}\right|^2 &= \left|\overline{\mathcal{M}}^{s_t}_{decay}\right|^2_{w_t\to\bar{w}_t}, \quad (7)
\end{aligned}$$

where the neglected terms are proportional to the virtuality $k_t^2-m_t^2$ of the top quark.

Below we focus on the first decay piece $\left|\overline{\mathcal{M}}^{s_t}_{decay}\right|^2$, which contributes to the LO polarized top-quark jet function $J_t^{s_t(0)}(m_{J_t}^2, E_{J_t}, R_t)$. After including QCD radiations, the top-jet

mass m_{J_t} (energy E_{J_t}) may differ from the top-quark mass m_t (energy E_t), i.e., the top-jet momentum k_{J_t} may differ from the top-quark momentum k_t. $J_t^{s_t(0)}$ can be factorized, as depicted in Fig. 2, by inserting the Fierz identity and by introducing the light-like vectors

$$\xi_b^\alpha \equiv \frac{1}{\sqrt{2}}(1,-\vec{n}_b), \qquad\qquad \bar{\xi}_b^\alpha \equiv \frac{1}{\sqrt{2}}(1,\vec{n}_b), \tag{8}$$

with the unit vector $\vec{n}_b$ being along the bottom-quark momentum. The identity for defining the bottom-quark jet function with the jet momentum k_{J_b} [4],

$$1 \;=\; \int dm_{J_b}^2 dE_{J_b} d^2\vec{n}_{J_b} \delta(m_{J_b}^2 - m_b^2)\delta(E_{J_b} - E_b)\delta^2(\vec{n}_{J_b} - \vec{n}_b), \tag{9}$$

is also inserted, where m_{J_b}, E_{J_b}, and $\vec{n}_{J_b}$ are the invariant mass, the energy, and the direction of the bottom jet, respectively, and E_b is the energy of the bottom quark. For factorization at higher orders in QCD, the bottom-quark mass m_b (energy E_b, direction $\vec{n}_b$) is replaced by the invariant mass (total energy, direction of total momentum) of all the partons in the bottom jet.

The LO polarized top-quark jet function is then written as

$$\begin{aligned} J_t^{s_t(0)}(m_{J_t}^2, E_{J_t}, R_t) \;=\; & \frac{(2\pi)^3}{4\sqrt{2}E_{J_t}} \int dm_{J_b}^2 dE_{J_b} d^2\vec{n}_{J_b} \frac{d^4k_\ell}{(2\pi)^3}\delta_+(k_\ell^2) d^4k_\nu \delta_+(k_\nu^2) \\ & \times H^{(0)}(k_{J_t}, k_{J_b}, k_\ell) J_b^{(0)}(m_{J_b}^2, E_{J_b}, R_b)\delta^4(k_{J_t} - k_{J_b} - k_\ell - k_\nu), \end{aligned} \tag{10}$$

with the LO top-quark decay kernel $H^{(0)}$ and the LO bottom-quark jet function $J_b^{(0)}$

$$\begin{aligned} H^{(0)}(k_{J_t}, k_{J_b}, k_\ell) \;=\; & 4C_{decay}A_b^{-1}(\xi_t \cdot k_{J_t})(k_\nu \cdot \bar{\xi}_b)\left[(k_\ell \cdot k_{J_t}) - m_t(k_\ell \cdot s_t)\right], \\ J_b^{(0)}(m_{J_b}^2, E_{J_b}, R_b) \;=\; & A_b \int \frac{d^4k_b}{(2\pi)^3}\delta_+(k_b^2 - m_b^2)\delta(m_{J_b}^2 - m_b^2)\delta(E_{J_b} - E_b)\delta^2(\vec{n}_{J_b} - \vec{n}_b) \\ & \times \mathrm{tr}\left[(\not{k}_b + m_b)\not{\xi}_b\right], \end{aligned} \tag{11}$$

R_b being the bottom-jet cone radius. The normalization constant $A_b = (2\pi)^3/(2\sqrt{2}E_{J_b}^2)$ is absorbed into $J_b^{(0)}$, such that $J_b^{(0)} = \delta(m_{J_b}^2 - m_b^2)$ holds after the integration over k_b is worked out. To arrive at Eq. (10), contributions down by powers of m_{J_b}/E_{J_b} have been ignored. The above factorization can be extended to all orders in QCD following the procedures outlined in [4], and we replace $J_t^{s_t(0)}$ ($J_b^{(0)}$) by its all-order definition $J_t^{s_t}$ (J_b). The choice $R_b = R_t$ is made, so that the bottom-quark jet function absorbs not only collinear radiations, but also soft radiations in the top jet. The remaining infrared finite radiations go into the hard top-quark decay kernel, which sticks to the LO expression below.

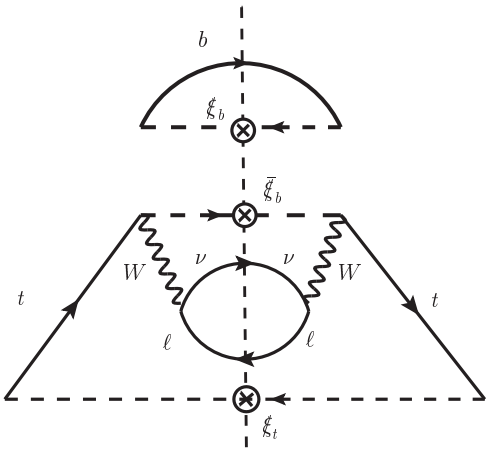

FIG. 2: LO factorization of the bottom-quark jet function from the polarized leptonic top. The symbols $\otimes$ represent the insertions of the gamma matrices $\not{\xi}_b$ and $\bar{\not{\xi}}_b$ from the Fierz identity.

The lepton kinematic variables are first integrated out in the rest frame of the top quark, leading to

$$J_t^{s_t}(m_{J_t}^2, \bar{E}_{J_t}, \bar{R}_t) = f_t(z_{J_t}) \int dz_{J_b} d\bar{x}_{J_b} d\cos\bar{\theta}_{J_b} \times \left[F_a(z_{J_t}, \bar{x}_{J_b}, z_{J_b}) + |\vec{s}_t| F_b(\bar{x}_{J_b}, z_{J_b}) \cos\bar{\theta}_{J_b}\right] J_b(m_{J_b}^2, \bar{E}_{J_b}, \bar{R}_t), \quad (12)$$

where $\bar{E}_{J_t} = m_{J_t}$, $\bar{E}_{J_b}$ is the bottom-jet energy in the rest frame, the dimensionless parameters z_{J_t}, $\bar{x}_{J_b}$, and z_{J_b} are defined as

$$z_{J_t} = \frac{m_{J_t}^2}{m_t^2}, \qquad \bar{x}_{J_b} = \frac{2\bar{E}_{J_b}}{m_{J_t}}, \qquad z_{J_b} = \frac{m_{J_b}^2}{m_{J_t}^2}, \quad (13)$$

$\bar{\theta}_{J_b}$ is the polar angle of the bottom-jet momentum relative to the top spin $\vec{s}_t$ (see Fig. 3 in Ref. [4]), and $\bar{R}_t$ is the upper bound of $\bar{\theta}_{J_b}$ in the rest frame. The hard functions F_a and F_b are given by

$$F_a(z_{J_t}, x_{J_b}, z_{J_b}) = \sqrt{z_{J_t}} x_{J_b} \beta_{J_b} f_W(x_{J_b}, z_{J_b}) \left(-\frac{1}{3}x_{J_b}^2 + \frac{1+z_{J_b}}{2}x_{J_b} - \frac{2}{3}z_{J_b}\right),$$
$$F_b(x_{J_b}, z_{J_b}) = f_W(x_{J_b}, z_{J_b}) \left[-\frac{1}{3}x_{J_b}^3 + \frac{1+3z_{J_b}}{6}x_{J_b}^2 + \frac{4}{3}z_{J_b}x_{J_b} - \frac{2}{3}z_{J_b}(1+3z_{J_b})\right], \quad (14)$$

with $\beta_{J_b} = \sqrt{1 - m_{J_b}^2/E_{J_b}^2}$, which coincide with Eq. (26) in the study of the spin analyzing power for a polarized top quark at rest [4], as the on-shell condition $z_{J_t} = 1$ is taken. That is, Eq. (12) can be regarded as a formula of the spin analyzing power for an off-shell top

quark. The functions f_t and f_W

$$\begin{aligned} f_t(z_{J_t}) &= \frac{1}{16\pi}|V_{tb}|^2 m_W^4 G_F^2 z_{J_t}^{3/2} \frac{1}{(1-z_{J_t})^2+\eta_t^2}, \\ f_W(x_{J_b}, z_{J_b}) &= \frac{1}{(1+z_{J_b}-x_{J_b}-\xi)^2+(\xi\eta)^2}, \end{aligned} \tag{15}$$

arise from the top-quark and W-boson propagators, respectively, with the Fermi constant G_F, and the dimensionless mass ratios

$$\eta_t = \frac{\Gamma_t}{m_t}, \qquad \xi = \frac{m_W^2}{m_{J_t}^2}, \qquad \eta = \frac{\Gamma_W}{m_W}. \tag{16}$$

The top-quark spin is chosen in the positive z-axis, $s_t^\mu = (0,0,0,1)$. We then boost the top-quark rest frame with a velocity parameter v_t along the negative z-axis to make a right-handed top quark ($v_t > 0$) or a left-handed top quark ($v_t < 0$) [34], with the absolute value $|v_t| = \sqrt{1-m_{J_t}^2/E_{J_t}^2}$. The jet energies E_{J_t} and E_{J_b}, and the polar angle θ_{J_b} of the bottom jet in the boosted frame are related to those in the rest frame of the top quark via the Lorentz transformation

$$\begin{aligned} \gamma_t \bar{E}_{J_t} &= E_{J_t}, \\ \bar{x}_{J_b} &= 2\gamma_t^2 x_{J_b}(1 - v_t \cos\theta_{J_b}), \\ \cos\bar{\theta}_{J_b} &= \frac{-v_t + \cos\theta_{J_b}}{1 - v_t\cos\theta_{J_b}}, \end{aligned} \tag{17}$$

with the gamma factor γ_t, and the bottom-jet energy fraction $x_{J_b} = E_{J_b}/E_{J_t}$. We have neglected the bottom-jet mass compared to the top-jet mass in Eq. (17), since this approximation holds well and renders our formalism simpler.

We then derive the right-handed top-quark jet function

$$\begin{aligned} J_t^R(m_{J_t}^2, E_{J_t}, R_t) &= f_t(z_{J_t}) \int_0^1 dz_{J_b} \int_{\cos R_t}^1 d\cos\theta_{J_b} \int_0^{J/(4\gamma_t^2)} dx_{J_b} \\ &\quad \times J\left[F_a(z_{J_t}, \bar{x}_{J_b}, z_{J_b}) + |\vec{s}_t| F_b(\bar{x}_{J_b}, z_{J_b})\cos\bar{\theta}_{J_b}\right] J_b(m_{J_b}^2, E_{J_b}, R_t), \end{aligned} \tag{18}$$

with the Jacobian $J = 2/(1 - v_t\cos\theta_{J_b})$ being from the Lorentz transformation. Note that the variables $\bar{x}_{J_b}$ and $\cos\bar{\theta}_{J_b}$ are understood as functions of x_{J_b} and $\cos\theta_{J_b}$ through Eq. (17). Moreover, we have replaced the bottom-quark jet function $J_b(m_{J_b}^2, \bar{E}_{J_b}, \bar{R}_t)$ in Eq. (12) by $J_b(m_{J_b}^2, E_{J_b}, R_t)$ in Eq. (18). The use of the former corresponds to the sequence of performing the factorization of the bottom-quark jet function in the top-quark rest frame, and then applying the boost, while the use of the latter corresponds to the sequence of applying

the boost first, and then performing the factorization. These two sequences are equivalent, because the jet function depends on the product $E_{J_b}R_b$, instead of on E_{J_b} and R_b separately, as observed in [32]. It can be shown by employing the Lorentz transformation in Eq. (17) that $E_{J_b}R_b$, which bears the meaning of the transverse momentum relative to the bottom-quark jet axis, is boost-invariant in the small R_b limit. Note that the factorization presented in this work and the resummation performed in [32] hold up to power corrections of R_b. In other words, the scaling of a jet function with the product of the jet energy and the jet cone radius is closely related to the commutability of the boost and factorization operations. The left-handed top-quark jet function J_t^L, as a consequence of the Lorentz transformation of $J_t^{\bar{s}_t}$, is easily obtained from J_t^R by flipping the sign of the second term, namely, $\cos\bar{\theta}_{J_b}$ in Eq. (18). We set $|s_t| = 1$ in the analysis below for a highly-boosted top quark.

According to Eq. (1), we count the contribution from a final-state parton to the top-quark jet energy function, if it is emitted into the test cone of radius r. It is assumed that the charged lepton can be identified and its contribution is excluded. The neutrino does not contribute either due to missing momentum. The LO factorization is applied to the expression $|\overline{\mathcal{M}}_{decay}|^2 E_{J_b}\theta(r-\theta_{J_b})$, which can be interpreted as the expectation value of the bottom-jet energy within the test cone. This step results in the LO bottom-quark jet energy function $J_b^{E(0)} = E_{J_b}\delta(m_{J_b}^2 - m_b^2)$. The factorization of QCD radiations gives, with the top-jet mass being integrated out, the right-handed top-quark jet energy function

$$\begin{aligned} J_t^{E,R}(E_{J_t}, R_t, r) \;=\; & \int_0^{\gamma^2} \frac{dz_{J_t}}{z_{J_t}} f_t(z_{J_t}) \int_{\cos r}^1 d\cos\theta_{J_b} \int_0^{J/(4\gamma_t^2)} dx_{J_b} \\ & \times J x_{J_b}^2 \left[F_a(z_{J_t}, \bar{x}_{J_b}, 0) + F_b(\bar{x}_{J_b}, 0)\cos\bar{\theta}_{J_b}\right] J_b^E(E_{J_b}, R_t, r), \end{aligned} \tag{19}$$

as the convolution of the hard functions F_a and F_b with the bottom-quark jet energy function $J_b^E(E_{J_b}, R_t, r)$. The smaller cone of radius r in the bottom jet is centered around the bottom-jet axis. The additional factor $x_{J_b}^2$ in the second line of the above expression arises from the different Mellin variables $m_{J_t}^2/(E_{J_t}R_t)^2$ for the left-hand side and $m_{J_b}^2/(E_{J_b}R_t)^2$ for the right-hand side. The bottom-jet mass dependence has been dropped in the hard functions due to its smallness compared to other mass scales. Therefore, the bottom-jet mass can be integrated out trivially, leading to the $N = 1$ moment of the bottom-quark jet energy function $J_b^E(E_{J_b}, R_t, r)$ in Eq. (19). The left-handed top-quark jet energy function $J_t^{E,L}$ is derived from $J_t^{E,R}$ by flipping the sign of $\cos\bar{\theta}_{J_b}$.

The lower bound $\cos r$ of $\cos\theta_{J_b}$ in Eq. (19) implies that the bottom jet does not contribute

to the top-jet energy profile, as the polar angle of the bottom-jet axis goes outside the test cone. However, the smaller cone in the bottom jet still overlaps with the test cone when θ_{J_b} is slightly greater than r, so the contribution from the bottom jet does not vanish sharply. How to count the partial contribution from the overlap region of the test cone of the top jet and the smaller cone of the bottom jet depends on a scheme, under which radiations in the former are factorized into the latter. Our goal in this work is to demonstrate the difference between the energy profiles of the left- and right-handed top jets. Hence, we do not intend to explore the sophisticated issue related to the factorization scheme, and assume vanishing of the bottom-jet contribution as $\theta_{J_b} > r$.

III. NUMERICAL ANALYSIS

It is easy to obtain the polarized top-quark jet functions at LO in QCD by substituting $\delta(m_{J_b}^2 - m_b^2)$ for the bottom-quark jet function J_b in Eq. (18). For the inclusion of QCD effects, we replace J_b in Eq. (18) by the light-quark jet function from the resummation formalism [32]. It is more convenient to employ the fitted expression in Eq. (29) of Ref. [4]. The following parameters [35] are adopted

$$\begin{aligned} m_b &= 4.18 \text{ GeV}, \qquad m_W = 80.39 \text{ GeV}, \qquad m_t = 172.5 \text{ GeV}, \\ G_F &= 1.16637 \times 10^{-5} \text{ GeV}^{-2}, \qquad \Gamma_W = 2.09 \text{ GeV}, \\ \Gamma_t^{\rm LO} &= 1.48 \text{ GeV}, \qquad \Gamma_t^{\rm NLO} = 1.33 \text{ GeV}, \end{aligned} \tag{20}$$

where the top-quark decay width $\Gamma_t^{\rm LO}$ is inserted into the function f_t for the analysis at LO, and the next-to-leading-order (NLO) one $\Gamma_t^{\rm NLO}$ [36] is inserted for the analysis with resummation.

The jet mass dependence of the normalized top-quark jet functions $J_t^{R,L}(m_{J_t}^2)/N$, $N = \int dm_{J_t}^2 [J_t^R(m_{J_t}^2) + J_t^L(m_{J_t}^2)]$, for the top-jet energy $E_{J_t} = 1$ TeV and cone radius $R_t = 0.7$ are displayed in Fig. 3. As mentioned before, the bottom-quark jet function demands that the dominant contribution arises from the region $m_{J_b} \sim O(m_b)$, which is much smaller than other mass scales, like the top-quark and W-boson masses. If the bottom-jet mass dependence is negligible in the hard kernel, the integration of the bottom-quark jet function over the bottom-jet mass can be performed trivially, giving a normalization constant. Therefore, the LO curves are close to those with the resummation effect. It has been numerically

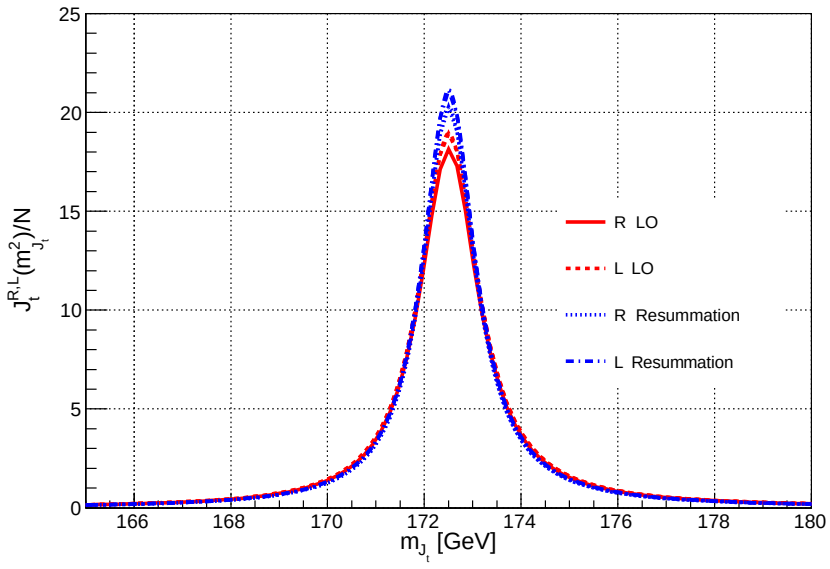

FIG. 3: Comparison between the LO results and those including the resummation effect for the polarized top-quark jet functions with $E_{J_t} = 1$ TeV and $R_t = 0.7$.

confirmed that the lower LO values around the peak position are mainly attributed to the top decay widths $\Gamma_t^{\rm LO} > \Gamma_t^{\rm NLO}$. It is also observed that the left-handed jet function is roughly the same as the the right-handed one, and slightly higher than the right-handed one at the peak position. It implies that the mass distributions of the left- and right-handed top jets, computed as the convolution of the parton-level production cross section with parton distribution functions and the polarized top-quark jet functions, will be basically identical. We have also investigated the behavior of the normalized top-quark jet functions for $E_{J_t} = 500$ GeV, 1 TeV, and 2 TeV and for $R_t = 0.4$, 0.7, and 1.0, which is similar to that shown in Fig. 3. The difference between the left- and right-handed top-quark jet functions decreases with E_{J_t} as expected.

We then focus on the energy profiles of the polarized top jets. For a top jet produced in $q\bar{q} \to t\bar{t}$ at central rapidity with a fixed top-jet energy, its energy profile is simply related to the jet energy function, because the production pieces, including the LO parton-level cross section and parton distribution functions, cancel in the ratios

$$R(r) \;=\; \frac{J_t^{E,R}(E_{J_t}, R_t, r)}{J_t^{E,R}(E_{J_t}, R_t, R_t)}, \qquad\qquad L(r) = \frac{J_t^{E,L}(E_{J_t}, R_t, r)}{J_t^{E,L}(E_{J_t}, R_t, R_t)}. \tag{21}$$

It is obvious that the above definitions for the right- and left-handed top-jet energy profiles

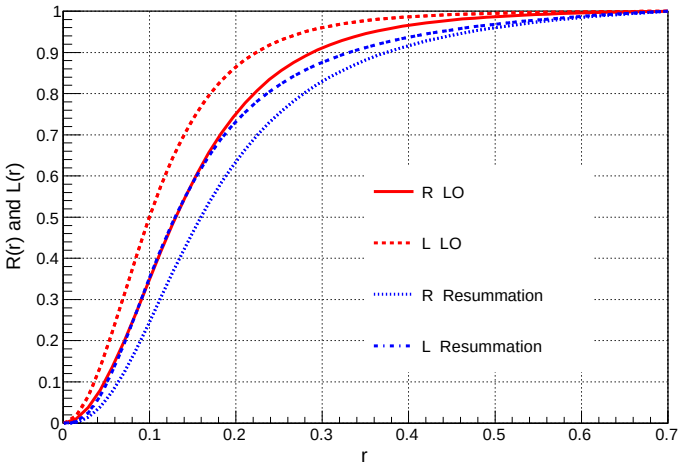

FIG. 4: Comparison between the LO results and those including the resummation effect for the energy profiles of the polarized top jets with $E_{J_t} = 1$ TeV and $R_t = 0.7$.

satisfy $R(r = 0) = L(r = 0) = 0$ and $R(r = R_t) = L(r = R_t) = 1$. We calculate the LO jet energy function $J_t^{E,R}$ for the right-handed top quark by substituting $J_b^{E(0)} = 1/E_{J_b}$ in the Mellin space for the bottom-quark jet energy function in Eq. (19). As verified above, the bottom-jet mass dependence in the factorization formula for the top-quark jet function is negligible. With this approximation, the analytical expressions for the LO top-quark jet energy functions can be derived, which are presented in the appendix.

The QCD effects are taken into account by adopting the bottom-quark jet energy function $J_b^E = (1/E_{J_b}) \exp[S_q(E_{J_b}, R_t, r)]$, which resums the double logarithm $\alpha_s \ln^2(r/R_t)$ to all orders [32]. The Sudakov exponent $S_q(E_{J_b}, R_t, r)$ is evaluated with the LO QCD running coupling. In principle, the NLO correction to the initial condition $1/E_{J_b}$ of the bottom-quark jet energy function should be included, which is acquired by matching the Sudakov exponent to the complete NLO contribution. However, this correction, without the large logarithm, is expected to be less crucial. The LO results of the energy profiles $R(r)$ and $L(r)$ and those from the QCD resummation for $E_{J_t} = 1$ TeV and $R_t = 0.7$ are compared in Fig. 4: the curves with the resummation are lower than the LO ones by 15% at $r = 0.2$, by 30% at $r = 0.1$, and by almost 100% as $r \to 0$. The QCD effects spread the bottom-quark energy into soft gluons, such that the energy is accumulated more slowly.

It is also noticed that the jet energy is accumulated faster in the left-handed top jet than

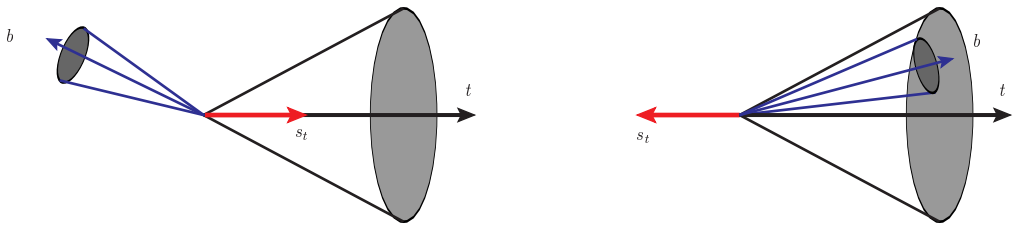

(a) (b)

FIG. 5: Pictorial explanation of the different energy profiles in the (a) right-handed and (b) left-handed top jets. The configuration (b) shows a larger probability for the bottom jet to go inside the top-jet cone due to the $V-A$ structure ($\kappa_b < 0$).

in the right-handed one. The mechanism is the same as that responsible for the higher mass distribution of the left-handed top jet, which can be understood via the $V-A$ structure of weak interaction. First, the spin analyzing power κ_i for decay product i of a polarized top quark in the rest frame is defined via the angular distribution [37, 38]

$$\frac{1}{\Gamma}\frac{d\Gamma}{d\cos\theta_i} = \frac{1}{2}(1+\kappa_i\cos\theta_i), \qquad i = b, \ell, \nu, \tag{22}$$

where $\Gamma = \Gamma(t \to b\ell\nu)$ is the partial decay width, and θ_i is the polar angle of the decay product momentum relative to the top spin. The spin analyzing powers for the bottom quark, the charged lepton, and the neutrino were found to be $\kappa_b \simeq -0.4$, $\kappa_\ell \simeq +1.0$, and $\kappa_\nu \simeq -0.3$ (see the Table 1 in [39] with the correspondence between the u quark and the neutrino, and between the $\bar{d}$ quark and the charged lepton). That is, the bottom quark and the neutrino tend to be emitted in the direction opposite, i.e., anti-correlated to the top spin, while the charged lepton tends to be correlated to the top spin. According to the definition of the helicity, the bottom quark, which tends to be emitted opposite to the top-quark momentum, has a higher chance to go outside the cone of a right-handed top jet as depicted in Fig. 5(a). Hence, the bottom jet gives less contribution to the right-handed top-jet mass and energy profile. For a boosted left-handed top quark, the favored configuration is the one with the bottom quark being emitted along the top-quark momentum, so the bottom jet has a higher chance to go inside the top-jet cone as shown in Fig. 5(b), and contributes more to the jet mass and energy profile. The difference between the energy fraction distributions of a particular subjet for the left- and right-handed top jets observed in [30] is also attributed to the same mechanism.

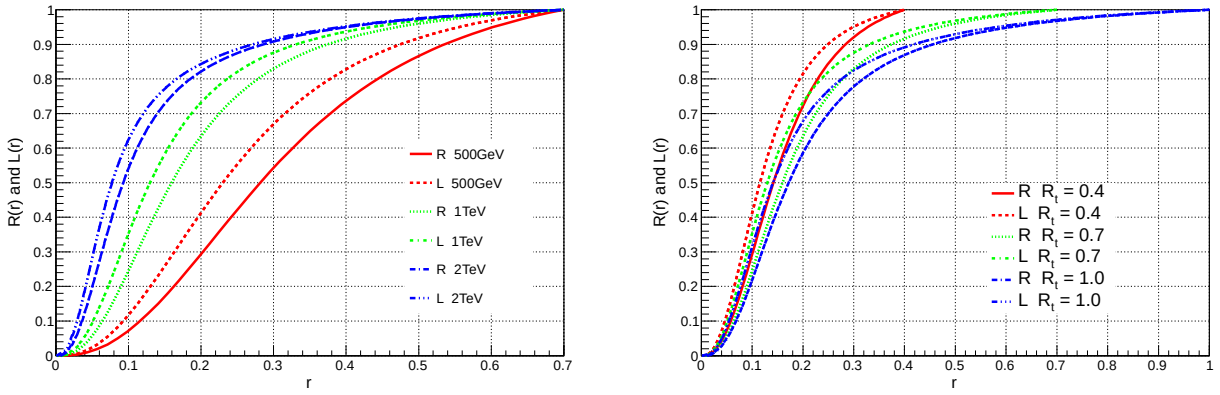

(a) (b)

FIG. 6: Dependencies of the top-jet energy profiles on (a) top-jet energy E_{J_t} for $R_t = 0.7$ and (b) top-jet cone radius R_t for $E_{J_t} = 1$ TeV.

The energy profiles $R(r)$ and $L(r)$ for various top-jet energies $E_{J_t} = 500$ GeV, 1 TeV, and 2 TeV and cone radii $R_t = 0.4$, 0.7, and 1.0 are presented in Fig. 6. For a typical transverse momentum (< 1 TeV) carried by a boosted top quark at LHC, $R(r)$ and $L(r)$ can differ by about 30% at small $r < 0.2$ as shown in Fig. 6(a), which is significant enough for experimental discrimination. As a top quark becomes highly boosted, the difference decreases as expected, since the bottom quark becomes collimated with the top quark more exactly. For example, the difference reduces to about few percent at $r = 0.2$ as the top-jet energy reaches $E_{J_t} = 2$ TeV for $R_t = 0.7$. Figure 6(b) indicates that the difference between $R(r)$ and $L(r)$ is not sensitive to the cone radius as $R_t > 0.7$. For $R_t = 0.4$, the difference drops to 10% at $r = 0.2$, and the energy profiles do not exhibit saturation in the whole range of r. It implies that this cone radius is too small to collect majority of the top-jet energy, and a cone radius larger than $R_t = 0.7$ is preferred for LHC measurements.

IV. CONCLUSION

In this paper we have studied the helicity dependence of the mass distribution and the energy profile as examples of jet substructures for a boosted polarized top quark. The former (latter) is factorized into the convolution of the hard top-quark decay kernel with the bottom-quark jet function (jet energy function). It has been found that the QCD effects

introduced by the bottom-quark jet function on the mass distribution of a polarized top jet are minor. Those introduced by the bottom-quark jet energy function on the top-jet energy profile are more significant, which lower the LO top-jet energy profile by 15% at $r = 0.2$ and by 30% at $r = 0.1$ for the top-jet energy $E_{J_t} = 1$ TeV and cone radius $R_t = 0.7$. The reduction is similar for the right- and left-handed top jets, since QCD interaction is vector-like, i.e., it is independent of the chirality of the top quark.

Both the jet mass distribution and the jet energy profile of the left-handed top jet are larger than those of the right-handed one for various top-jet energies and cone radii. This observation is a consequence of the $V - A$ structure of weak interaction, under which the favored direction of the emitted bottom quark is opposite to the top spin. However, the mass distribution is not sensitive to the helicity, but the energy profile is: energy is accumulated faster within the left-handed top jet than within the right-handed one. The difference is about 30% at small r with a larger top-jet cone $R_t > 0.7$ for typical boosted top quarks at LHC. The measurement of the neutrino missing momentum, the b-tagging, and the W-reconstruction are not required for this observable. That is, the energy profile is a simple and useful jet substructure for helicity discrimination of a boosted top quark, which can help identification of new physics beyond the Standard Model at LHC.

We expect differences in other jet substructures of the left- and right-handed top jets. A straightforward application of our formalism is to study the leptonic energy distributions, whose difference between the left- and right-handed top jets is also related to the $V - A$ structure of weak interaction. We will extend our formalism to analysis of jet substructures of a boosted hadronically decaying top quark. In addition to the factorization of QCD radiations into three light-quark jets, a soft function, which collects soft gluon exchanges among the three final-state light quarks, needs to be introduced. The behavior of this soft function can be extracted through the resummation technique in the manner the same as for the light-particle jet functions [32]. The energy profile of a hadronically decaying top jet can then be predicted.

Acknowledgment

YK thanks H. Yokoya and members of physics departments at Hiroshima university and Toyama university for useful discussions. This work was supported in part by the National

Science Council of R.O.C. under Grant No. NSC-101-2112-M-001-006-MY3, and by the National Center for Theoretical Sciences of R.O.C..

Appendix A: LO TOP JET ENERGY FUNCTIONS

We compute the LO jet energy function $J_t^{E,R}$ for the right-handed top quark by substituting $1/E_{J_b}$ for the bottom-quark jet energy function J_b^E in Eq. (19). Neglecting the bottom-jet mass dependence, we have

$$J_t^{E,R}(E_{J_t}, R_t, r) \;=\; f_t^E \left[\left(\frac{1}{2} I_3 - \frac{1}{3} I_4 \right) A(E_{J_t}, r) + \left(\frac{1}{6} I_3 - \frac{1}{3} I_4 \right) B(E_{J_t}, r) \right], \qquad \text{(A1)}$$

with the constant

$$f_t^E = \frac{1}{32} \frac{1+v_t^2}{\gamma_t^4 R_t E_{J_t} \eta_t} G_F^2 m_W^4 |V_{tb}|^2. \qquad \text{(A2)}$$

The functions

$$\begin{aligned} A(E_{J_t}, r) \;&=\; \frac{1}{2} \frac{(1-\cos r)[2 - v_t(1+\cos r)]}{(1-v_t)^2 (1 - v_t \cos r)^2}, \\ B(E_{J_t}, r) \;&=\; \frac{1}{6 v_t^2} \left[\frac{(-1+2v_t)}{(1-v_t)^2} + \frac{1 - 3 v_t \cos r + 2 v_t^2}{(1 - v_t \cos r)^3} \right], \end{aligned} \qquad \text{(A3)}$$

come from the integration over the polar angle of the bottom jet. The functions

$$\begin{aligned} I_3 \;=\; & \frac{5}{2} - 2\xi + \frac{1-\xi}{\xi\eta} \left[(1-\xi)^2 - 3(\xi\eta)^2 \right] \left[\tan^{-1}\left(\frac{1}{\eta} \right) - \tan^{-1}\left(\frac{1}{\eta}\left(1 - \frac{1}{\xi} \right) \right) \right] \\ & + \frac{1}{2} \left[3(1-\xi)^2 - (\xi\eta)^2 \right] \ln \left[\frac{1+\eta^2}{(1-1/\xi)^2 + \eta^2} \right], \\ I_4 \;=\; & \frac{1}{3} \left[1 + 3(1-\xi) + 9(1-\xi)^2 - 3(\xi\eta)^2 \right] \\ & + \frac{1}{\xi\eta} \left[(1-\xi)^4 - 6(1-\xi)^2 (\xi\eta)^2 + (\xi\eta)^4 \right] \left[\tan^{-1}\left(\frac{1}{\eta} \right) - \tan^{-1}\left(\frac{1}{\eta}\left(1 - \frac{1}{\xi} \right) \right) \right] \\ & + 2(1-\xi) \left[(1-\xi)^2 - (\xi\eta)^2 \right] \ln \left[\frac{1+\eta^2}{(1-1/\xi)^2 + \eta^2} \right], \end{aligned} \qquad \text{(A4)}$$

are results of the integration over the bottom-jet energy, where the subscripts 3 and 4 in I_3 and I_4 refer to the powers of $\bar{x}_{J_b}$ in the integrands. The narrow-width approximation has been applied to the top-quark propagator, as performing the z_{J_t} integration. The LO jet energy function $J_t^{E,L}$ for the left-handed top quark is derived by flipping the sign of the

second term in Eq. (A1).

---

[1] W. Bernreuther, J. Phys. G **35**, 083001 (2008).

[2] F.-P. Schilling, Int. J. Mod. Phys. A **27**, 1230016 (2012).

[3] J. M. Campbell and R. Keith Ellis, arXiv:1204.1513.

[4] Y. Kitadono and H.-n. Li, Phys. Rev. D **87**, 054017 (2013).

[5] W. Bernreuther, P. Gonzalez, and C. Mellein, arXiv:1401.5930.

[6] A. Ferroglia, B. D. Pecjak, and L. L. Yang, Phys. Rev. D **86**, 034010 (2012).

[7] A. Ferroglia, B. D. Pecjak, and L. L. Yang, JHEP **1210**, 180 (2012).

[8] B. Auerbach, S. V. Chkanov, and N. Kidonakis, arXiv:1301.5810.

[9] A. Ferroglia, S. Marzani, B. Pecjak, and L. L. Yang, JHEP **1401**, 028 (2014).

[10] B. Bhattacherjee, M. Guchait, S. Raychaudhuri, and K. Sridhar, Phys. Rev. D. **82**, 055006 (2010).

[11] P. Bandyopadhyay and B. Bhattacherjee, Phys. Rev. D **84**, 035020 (2011).

[12] T. Plehn, M. Spannowsky, and M. Takeuchi, JHEP **1105**, 135 (2011).

[13] K. Blum *et al.*, Phys. Lett. B **702**, 364-369 (2011).

[14] M. Perelstein and A. Spray, JHEP **1109**, 008 (2011).

[15] J. Berger, M. Perelstein, M. Saelim, and A. Spray, arXiv.1111.6594.

[16] B. Bhattacherjee, S. K. Mandal, and M. Nojiri, JHEP **1303**, 105 (2013).

[17] A. Chakraborty, D. K. Ghosh, D. Ghosh, and D. Sengupta, JHEP **1310**, 122 (2013).

[18] D. Duffty and Z. Sullivan, arXiv:1307.1820.

[19] A. Azatov, M. Salvarezza, M. Son, and M. Spannowsky, arXiv:1308.6601.

[20] J. Thaler and L.-T. Wang, JHEP **0807**, 092 (2008).

[21] D. E. Kaplan, K. Rehermann, M. D. Schwartz, and B. Tweedie, Phys. Rev. Lett. **101**, 142001 (2008).

[22] K. Rehermann and B. Tweedie, JHEP **1103**, 059 (2011).

[23] J. Thaler and K. V. Tiburg, JHEP **1202**, 093 (2012).

[24] C. Chen, Phys. Rev. D.**87**, 074007 (2013).

[25] C. Chen, Phys. Rev. D.**88**, 074009 (2013).

[26] S. Schätzel and M. Spannowsky, Phys. Rev. D **89**, 014007 (2014).

[27] M. Backovic, O. Gabizon, J. Juknevich, G. Perez, and Y. Soreq, arXiv:1311.2962.

[28] J. Pilot, EPJ Web. Conf. **60**, 09003 (2013).

[29] S. Fleischmann, J. Phys. Conf. Ser. **452**, 012034 (2013).

[30] D. Krohn, J. Shelton, and L.-T. Wang, JHEP **1007**, 041 (2010).

[31] L. G. Almeida, S. J. Lee, G. Perez, I. Sung, and J. Virzi, Phys. Rev. D **79**, 074012 (2009).

[32] H.-n. Li, Z. Li, and C. P. Yuan, Phys. Rev. Lett. **107**, 152001 (2011); Phys. Rev. D **87**, 074025 (2013).

[33] D. E. Acosta *et al.* (CDF Collaboration), Phys. Rev. D **71**, 112002 (2005).

[34] J. Shelton, Phys. Rev. D **79**, 014032 (2009).

[35] J. Beringer *et al.*, Phys. Rev. D **86**, 010001 (2012).

[36] M. Jezabek and J. H. Kühn, Nucl. Phys. **B314**, 1 (1989).

[37] M. Jezabek and J. H. Kühn, Nucl. Phys. **B320**, 20 (1989).

[38] A. Czarnecki, M. Jezabek, and J. H. Kühn, Nucl. Phys. **B351**, 70 (1991).

[39] A. Brandenburg, Z. G. Si, and P. Uwer, Phys. Lett. B **539**, 235 (2002).